J Supercond Nov Magn (2018) 31:1209–1217
DOI 10.1007/s10948-017-4307-y

ORIGINAL PAPER

Evolution of the Fe^{3+} Ion Local Environment During the Phase Transition ε-$Fe_2O_3 \rightarrow \alpha$-$Fe_2O_3$

S. S. Yakushkin[1,2,3] · D. A. Balaev[3] · A. A. Dubrovskiy[3] · S. V. Semenov[3] · K. A. Shaikhutdinov[3] · M. A. Kazakova[1,2] · G. A. Bukhtiyarova[1,3] · O. N. Martyanov[1,2,3] · O. A. Bayukov[3]

Received: 10 August 2017 / Accepted: 19 August 2017 / Published online: 31 August 2017

Abstract Evolution of the local environment of Fe^{3+} ions in deposited Fe_2O_3/SiO_2 nanoparticles formed in samples with different iron contents was investigated in order to establish the conditions for obtaining the stable ε-Fe_2O_3/SiO_2 samples without impurities of other iron oxide polymorphs. Microstructure of the samples with an iron content of up to 16% is studied by high-resolution transmission electron microscopy, X-ray diffraction analysis, and Mössbauer spectroscopy, and their magnetic properties are examined. At iron concentrations below 6%, calcinations of iron-containing precursor nanoparticles in a silica gel matrix lead to the formation of the ε-Fe_2O_3 iron oxide polymorphic modification without foreign phase impurities, while at the iron concentration in the range of 6–12%, the hematite phase forms in the sample in the fraction of no more than 5%. It is concluded on the basis of the data obtained that the spatial stabilization of iron-containing particles is one of the main factors facilitating the formation of the ε-Fe_2O_3 phase in a silica gel matrix without other iron oxide polymorphs. It is demonstrated that the increase in the iron content leads to the formation of larger particles in the sample and gradual changes of the Fe^{3+} ion local environment during the phase transition ε-$Fe_2O_3 \rightarrow \alpha$-$Fe_2O_3$.

✉ S. S. Yakushkin
stas-yk@catalysis.ru

[1] Boreskov Institute of Catalysis, Novosibirsk, Lavrentieva 5, 630090 Russia

[2] Novosibirsk State University, Novosibirsk, 630090 Russia

[3] Kirensky Institute of Physics, Federal Research Center KSC SB RAS, Krasnoyarsk, 660036 Russia

Keywords $\varepsilon-Fe_2O_3$ iron oxide nanoparticles · Phase transition · Structure size effect · Magnetic properties · Mossbauer spectroscopy

1 Introduction

Systems based on nanoparticles with the large specific surface are used in various physicochemical and catalytic processes as hydrocarbon crude sorbents for oil spill containment [1], highly active selective catalysts of heterogeneous chemical reactions [2–4], materials for biomedicine [5, 6], etc.

One of the factors determining the progress in nanotechnology is the occurrence of new properties at the transition to the nanoscale (size effect) [7]. The size effect in nanoparticles is often related to an increase in the fraction of surface atoms. A typical example of the structural size effect is the formation of ε-Fe_2O_3 iron oxide. According to the structure and fraction of four-coordinate cations, this phase is intermediate between the γ-Fe_2O_3 and α-Fe_2O_3 oxide phases [8]. Its structure and magnetic properties were established only in 1998 [9]. The ε-Fe_2O_3 phase is stable only in the form of nanoparticles because of its low surface energy [10] and passes to the α-Fe_2O_3 phase with increasing size [11]. The ε-Fe_2O_3 phase is attractive, first of all, due to its unique magnetic properties, including the extraordinarily high coercivity [12] and the occurrence of a magnetic phase transition at a temperature of 120 K [13–15].

At the same time, the stability of the ε-Fe_2O_3 phase observed only on nanoscale significantly complicates investigations of the systems based on it [16]. Despite the great number of available ε-Fe_2O_3 nanoparticle fabrication techniques [17–21], until recently, there are attempts to form a ε-Fe_2O_3 iron oxide-based system without impurities of other polymorphs have been unsuccessful [22].

According to Tuček et al. [22], the ε-Fe_2O_3 iron oxide is most frequently met in the mixture with the α-Fe_2O_3 and γ-Fe_2O_3 oxides. Sakurai et al. [11] and Ohkoshi et al. [23] attributed the instability of ε-Fe_2O_3 nanoparticles with a size over a certain critical value to the low surface energy of the ε-Fe_2O_3 iron oxide. Using the proposed model, the researches obtained ε-Fe_2O_3 particles of more than 100 nm in diameter [20] and even nanowires with a length of up to 2 μm [18, 24].

The study of the problem on stability of deposited ε-Fe_2O_3 nanoparticles at high temperatures showed [25] that the phase transitions between polymorphs are also size-dependent and the critical size changes with increasing temperature.

El Mendili et al. [26] studied the processes occurring in a system of deposited iron oxide nanoparticles upon their heat treatment. Depending on the total amount of iron oxide nanoparticles in a silica gel matrix, the structural transition to the thermodynamically stable α-Fe_2O_3 phase upon heat treatment of γ-Fe_2O_3 nanoparticles can occur with or without ε-Fe_2O_3 formation. Thus, we may conclude that in studying the properties of deposited iron oxide nanoparticles and structural transitions between different polymorphs, the local nanoparticle concentration in a silica gel matrix and the possibility of mass transfer between nanoparticles play a key role.

Nikolić et al. [27, 28] examined the interplay between the magnetic characteristics of a system of iron oxide nanoparticles in a silica gel matrix formed by sol-gel synthesis combined with a microemulsion technique and the heat treatment conditions. The authors gradually changed the conditions of heat treatment of the samples and established the correlation between the synthesis and heat treatment conditions and size characteristics of iron oxide nanoparticles and phase composition of a system. They found that during heat treatment of deposited ε-Fe_2O_3 nanoparticle systems, both the size and magnetic characteristics of the iron oxide phase change and, after a certain critical temperature, the agglomeration processes lead to the occurrence of α-Fe_2O_3 nanoparticles in a sample. Therefore, we may conclude that the formation of nanoparticles and conditions of their synthesis are extremely important in studying the systems based on ε-Fe_2O_3 nanoparticles in a silica gel matrix.

In this work, we synthesized and studied the samples of Fe_2O_3 nanoparticles deposited onto silica gel with different iron oxide contents. At the low (3 wt%) iron ion concentration in the samples, we observed the formation of ε-Fe_2O_3 nanoparticles with the narrow size distribution, which do not contain impurities of other polymorphs [29–31].

Studies of the magnetic properties of such systems [31–35] showed that the size characteristics of the deposited ε-Fe_2O_3 nanoparticles are important for forming their magnetic properties. In the system of ultrasmall (< 5 nm) deposited ε-Fe_2O_3/SiO_2 particles, the observed coercivity is much lower than that in the samples consisting of larger nanoparticles [31]. To establish the dependence of the magnetic properties on the deposited ε-Fe_2O_3 nanoparticle size, we compared the deposited iron oxide nanoparticles in the samples with different iron oxide contents. It was found that the increase in the iron content leads not only to the coercivity growth but also to the formation of nanoparticles with the α-Fe_2O_3 structure in the system. To follow the evolution of the Fe^{3+} ion local environment at the phase transition ε-$Fe_2O_3 \rightarrow \alpha$-$Fe_2O_3$, the samples with different ion contents were thoroughly studied by Mössbauer spectroscopy.

2 Experimental

The technique for forming ε-Fe_2O_3 nanoparticles includes (i) incipient wetness impregnation of a ChemAnalyt KSKG silica gel with a specific surface of 287 m^2/g, an average pore diameter of ∼140 Å, a pore volume of ∼0.35 cm^3/g, and a grain size of 0.25–0.5 mm with the aqueous solution of iron(II) sulfate heptahydrate (ACS, 99+%, CAS 7782-63-0); (ii) drying at a temperature of 110 °C for 4 h; and (iii) annealing at a temperature of 900 °C for 4 h in air. To increase the iron mass content, stages (i) and (ii) were multiply repeatedly. The iron mass contents in the investigated samples, designations of the latter, the number of impregnations at stages (i) and (ii), and average particle size (d) are given in Table 1. The α-Fe_2O_3 phase concentration was determined by Mössbauer spectroscopy.

High-resolution transmission electron microscopy (HRTEM) images were obtained on a JEOL JEM-2010 microscope at an accelerating voltage of 200 kV and a resolution of 1.4 Å. X-ray diffraction (XRD) study was carried out on an X'TRA powder diffractometer (Switzerland) in Cu Kα radiation at a wavelength (λ) of 1.5418 Å, a 2θ scanning step of 0.050, and a point accumulation time of 3 s. Mössbauer spectra of the samples were measured on an MC 1104Em spectrometer with a ^{57}Co(Cr) source at room

Table 1 Designations and parameters of a sample series containing ε-Fe_2O_3 nanoparticles

Sample	Number of impregnations	Fe content, wt%	d, nm	[C] α-Fe_2O_3, at.%
05FS	1	0.74	3.4	–
3FS	1	3.4	3.8	–
6FS	1	5.6	8.6	5
8FS	2	8	18.5	3
12FS	3	12.5	16.9	4
16FS	5	16.5	22.8	35

temperature. The magnetic properties were investigated on a vibrating sample magnetometer. Experimental magnetic moments were normalized to the Fe_2O_3 mass.

3 Results and Discussion

3.1 Microscopy and X-ray Diffraction Analysis

The synthesized samples were characterized by HRTEM and XRD techniques. According to the HRTEM data, samples 05FS and 3FS calcinated at 900 °C contain deposited iron oxide particles with a characteristic size of ∼4 nm and a narrow size distribution (Δd) of ∼2 nm. As was shown by Bukhtiyarova et al. [30] and Dubrovskiy et al. [35] using a set of XRD and Mössbauer spectroscopy data, during calcination of such samples, ε-Fe_2O_3 iron oxide nanoparticles without impurities of other polymorphs are formed. The interplanar spacings measured by HRTEM are consistent with the ε-Fe_2O_3 phase parameters (Fig. 1) and confirm the absence of other polymorphs in the samples with an iron content below 7% [30, 35]. At the same time, samples 8FS, 12FS, and 16FS with the high iron content (see HRTEM images in Fig. 1d–f) contain also iron oxide nanoparticles with the interplanar spacings typical of the α-Fe_2O_3 structure.

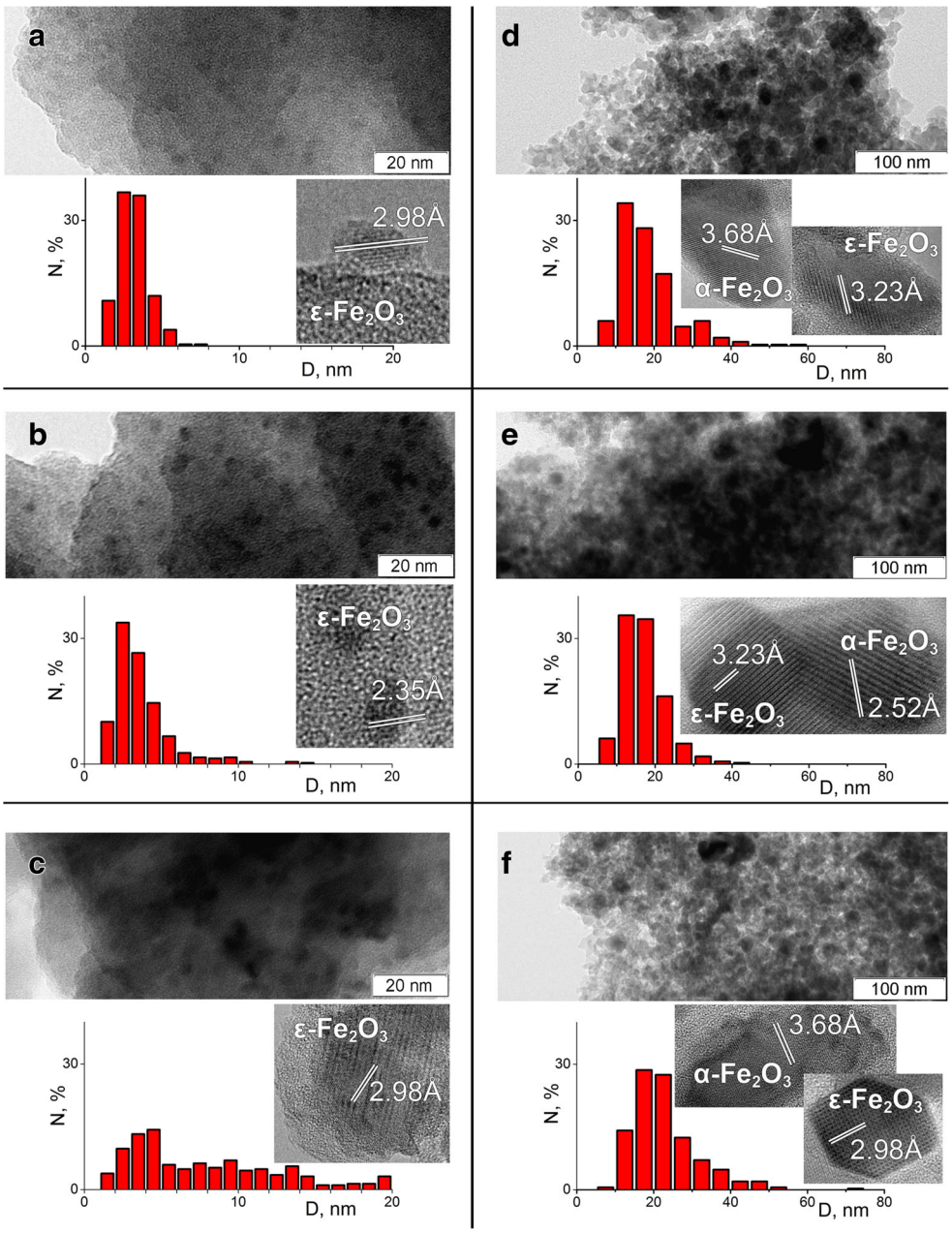

Fig. 1 HRTEM data and particle size distribution histograms for samples **a** 05FS, **b** 3FS, **c** 6FS, **d** 8FS, **e** 12FS, and **f** 16FS

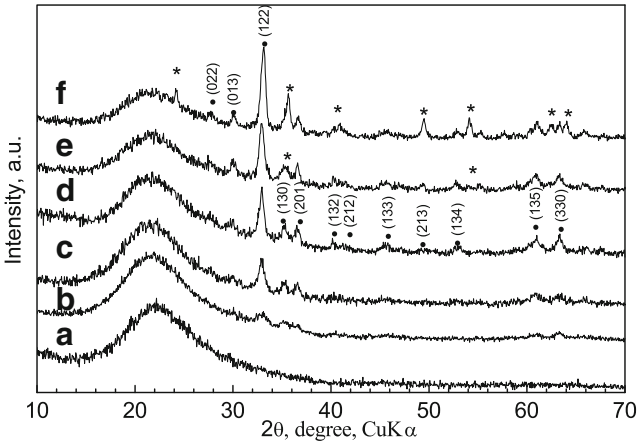

Fig. 2 Room-temperature XRD spectra of the ε-Fe_2O_3/SiO_2 samples with different iron ion contents: **a** sample 05FS, **b** sample 3FS, **c** sample 6FS, **d** sample 8FS, **e** sample 12FS, and **f** sample 16FS

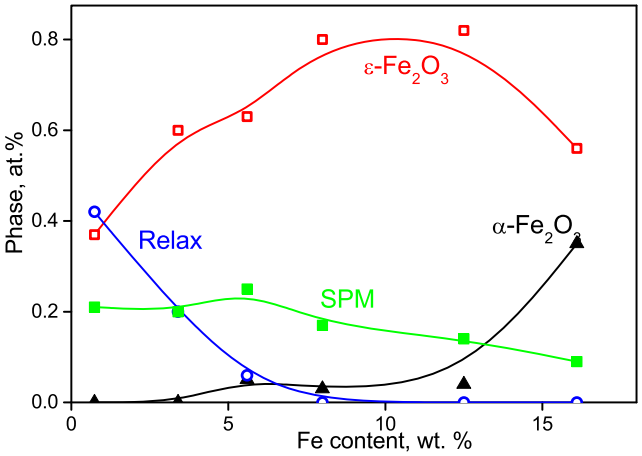

Fig. 4 Relative content of the Mössbauer spectrum components vs total iron ion content in the system

Analysis of the HRTEM size distribution of particles (Fig. 1) suggests a gradual increase in the average particle size at the transition to the samples with the high iron content. It can be clearly seen that the size distribution width significantly grows with increasing iron content. Already in sample 6FS, we observed an increase in the fraction of nanoparticles larger than 10 nm, which were formed via agglomeration of nanoparticles during the high-temperature heat treatment. With a further increase in the iron content, the average particle size sharply grows and nanoparticles with a size of no smaller than 20 nm are formed during redistribution of Fe^{3+} ions (see Table 1 and Fig. 1). The formation of such coarse particles and agglomerates in the samples results in the occurrence of the α-Fe_2O_3 iron oxide polymorphic modification impurity.

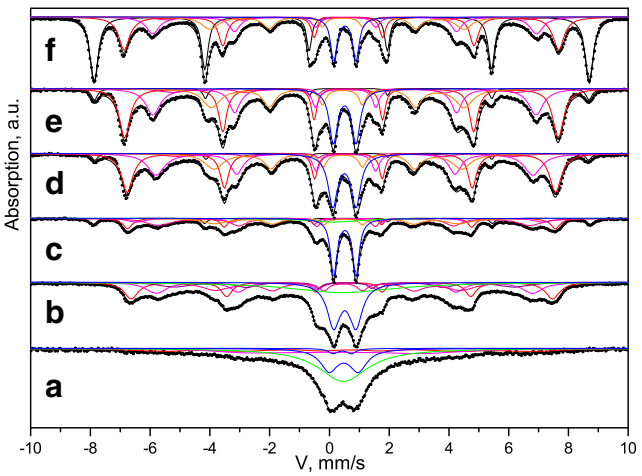

Fig. 3 Room-temperature Mössbauer spectra of samples **a** 05FS, **b** 3FS, **c** 6FS, **d** 8FS, **e** 12FS, and **f** 16FS (dots). The partial spectral components are also shown

Figure 2 shows XRD spectra of the samples with different iron contents. The broad component with the maximum near 22° in the spectra of all the samples corresponds to the amorphous SiO_2 substrate. The spectra of the samples with an iron content of < 6 wt% contain no sharp crystallographic reflections that could be attributed to any iron oxide, including ε-Fe_2O_3, which is related to the strong peak broadening typical of the systems of deposited nanoparticles smaller than 10 nm. As the iron content increases to 6%, the ε-Fe_2O_3 phase is reliably detected in the sample.

According to the HRTEM data, this sample contains ε-Fe_2O_3 nanoparticles of ~20 nm in size [35]. The occurrence of nanoparticles with such a size is apparently related to sintering and agglomeration of nanoparticles on the silica gel surface. When a sample contains ε-Fe_2O_3 nanoparticles larger than 10 nm, the phase can be identified by the XRD technique.

The increase in the iron content leads to the occurrence of the α-Fe_2O_3 crystallographic reflections in the spectrum. When the iron ion concentration in the sample attains 16 wt%, the α-Fe_2O_3 nanoparticle fraction is about 30% of the total iron oxide phase. Thus, as the iron content is increased, first, the size of nanoparticles increases due to their agglomeration and, then, the ε-Fe_2O_3 oxide transforms to hematite.

3.2 Mössbauer Spectroscopy

Evolution of the phase composition and local environment of iron ions in the samples containing simultaneously nanoparticles of two iron oxide polymorphic modifications (ε-Fe_2O_3 and α-Fe_2O_3) was examined by Mössbauer spectroscopy (see the results in Figs. 3 and 4 and Table 2).

The room-temperature Mössbauer spectra are the sum of Zeeman sextets and quadrupole doublets. The sextets correspond to the iron atoms in the magnetically ordered state.

Table 2 Mössbauer parameters of the spectra

	IS	H	QS	W_{34-16}	A	Position
05FS	0.45	386	−0.29	1.15–2.46	0.17	B1-B2
	0.27	272	−0.49	2.44–2.49	0.20	B3-A
	0.32	–	0.97	0.69	0.19	SPM-B
	0.28	–	0.61	0.37	0.02	SPM-A
	0.31	–	–	2.00	0.42	Relax
3FS	0.38	439	−0.46	0.32–0.57	0.17	B1
	0.39	392	−0.19	0.42–0.81	0.16	B2
	0.35	354	−0.08	0.33–1.24	0.11	B3
	0.22	255	−0.34	0.37–1.13	0.16	A
	0.36	–	0.74	0.52	0.20	SPM
	0.29	–	–	4.27	0.20	Relax
6FS	0.37	518	−0.45	0.16–0.26	0.05	$\alpha-Fe_2O_3$
	0.36	446	−0.44	0.21–0.38	0.13	B1
	0.35	424	−0.67	0.20–0.70	0.09	B2
	0.37	387	−0.13	0.29–0.98	0.24	B3
	0.19	254	−0.45	0.27–0.96	0.17	A
	0.36	–	0.75	0.26	0.25	SPM
	0.06	–	–	2.00	0.06	Relax
8FS	0.38	514	−0.48	0.12–0.22	0.03	$\alpha-Fe_2O_3$
	0.36	446	−0.47	0.24–0.46	0.31	B1
	0.37	393	−0.01	0.28–0.69	0.25	B2
	0.37	352	−0.02	0.25–1.04	0.05	B3
	0.21	258	−0.33	0.29–0.74	0.19	A
	0.35	–	0.77	0.38	0.17	SPM
12FS	0.37	516	−0.46	0.13–0.24	0.04	$\alpha-Fe_2O_3$
	0.36	452	−0.46	0.23–0.43	0.32	B1
	0.37	399	−0.08	0.28–0.59	0.24	B2
	0.36	359	−0.02	0.25–1.06	0.06	B3
	0.20	263	−0.31	0.28–0.70	0.20	A
	0.36	–	0.76	0.33	0.14	SPM
16FS	0.37	516	−0.43	0.21–0.32	0.35	$\alpha-Fe_2O_3$
	0.36	452	−0.47	0.24–0.44	0.24	B1
	0.37	400	−0.06	0.29–0.54	0.15	B2
	0.37	371	−0.08	0.20–0.71	0.04	B3
	0.19	265	−0.37	0.28–0.65	0.13	A
	0.36	–	0.74	0.26	0.09	SPM

IS is the isomer shift relative to α-Fe (±0.01 mm/s), H is the hyperfine field on the iron nucleus (±3 kOe), QS is the quadrupole splitting (±0.02 mm/s), W_{34-16} are the widths of internal (34) and external (16) sextet lines (±0.02 mm/s), and A is the fractional area under the partial spectrum (±0.03)

The doublets can be attributed to superparamagnetic nanoparticles in which the magnetic moment relaxation time is shorter than the nuclear spin relaxation time ($\sim 10^{-8}$ s), which results in hyperfine field averaging on a nucleus to zero.

The spectrum of sample 05FS is approximated by two Zeeman sextets with the very wide absorption lines and two quadrupole doublets, which can be attributed to the octahedral and tetrahedral oxide positions in accordance with their chemical shifts. The singlet should describe the relaxation component of the spectrum, which is caused by iron cations with the magnetic moment relaxation time comparable with the nuclear spin relaxation time. At room temperature, it is difficult to reliably identify the local environment of iron ions and phase composition of the nanosized phase by Mössbauer spectroscopy. However, as was shown in [35], the Mössbauer spectrum of this sample at a temperature of 4.2 K contains a sextet of lines with the parameters of the ε-Fe_2O_3 phase. We may state that the local environment of iron ions in oxide nanoparticles in this sample corresponds to the ε-Fe_2O_3 phase.

In the spectrum of sample 3FS, one can easily distinguish four sextets corresponding to the ε-Fe_2O_3 crystallographic positions. The strong broadening of the external sextet lines over the internal lines is observed, which is caused by inhomogeneity of the magnetic environment of the corresponding iron positions in oxide crystallites. The occupancy of the relaxation and superparamagnetic spectral components sharply decreased as compared with sample 05FS.

The intensity of the sextet corresponding to the α-Fe_2O_3 hematite phase occurs in sample 6FS and monotonically increases in the next samples, while the relative intensity of the relaxation and superparamagnetic components continues to decrease.

In the system of deposited ε-Fe_2O_3 nanoparticles, one can observe the formation of the paramagnetic (spin glass-like) subsystem on the surface of ε-Fe_2O_3 nanoparticles smaller than 6 nm [35]. Thus, when interpreting the Mössbauer spectroscopy data, the relaxation singlet can be attributed to iron ions on the surface of ε-Fe_2O_3 nanoparticles of 6 nm in size and smaller. It can be seen in Fig. 4 that the relative intensity of this Mössbauer spectrum component rapidly decreases at the transition to the samples with the high iron content, which is consistent with the TEM data (Fig. 1) showing that the average iron oxide nanoparticle size grows with the total iron content in the system [34, 35].

Figure 4 shows the evolution of the percent (at.% of iron) ratio between the observed Mössbauer positions of iron ions at the transition to the samples with the higher iron content.

Thus, the XRD and Mössbauer spectroscopy data are in good agreement and confirm that after calcination at a temperature of 900 °C, the ε-Fe_2O_3 particles form on the silica gel surface if the iron content is no higher than 6 wt%. With a further increase in the iron content in the sample after the sequential impregnations, one can observe, along with ε-Fe_2O_3 particles, the α-Fe_2O_3 phase on the sample surface. For the sample series under study, we can determine the iron concentration in the sample (6–8 wt%) at which the phase transition of ε-Fe_2O_3 nanoparticles to α-Fe_2O_3 ones occurs. However, only at the twofold higher

concentration, the α-Fe_2O_3 phase content in the sample sharply grows. Assuming that the phase transition ε-Fe_2O_3 $\rightarrow$ α-Fe_2O_3 occurs in particles with the largest size and using the HRTEM data on the size distribution (Fig. 1), we can estimate the critical size at which this phase transition occurs. For samples 6FS–12FS, the estimation yields a too large error, since the α-Fe_2O_3 phase content in these samples is small. For sample 16FS, where the α-Fe_2O_3 phase content is 35% according to the Mössbauer spectroscopy data, the calculation leads to a value of 38 $\pm$ 2 nm. Thus, the critical size of the structural phase transition ε-Fe_2O_3 $\rightarrow$ α-Fe_2O_3 caused by agglomeration of deposited iron oxide nanoparticles during synthesis is 35–40 nm.

3.3 Magnetic Properties

Figure 5 presents temperature dependences of the magnetic moment, $M(T)$, for samples 6FS, 8FS, 12FS, and 16FS in the range from 4.2 K to room temperature obtained upon zero-field cooling (ZFC mode) and in a field of 1 kOe (FC mode). The bright anomaly accompanied by the maximum near 130 K and the subsequent sharp decrease in the magnetic moment with a decrease in temperature to ~80 K corresponds to the well-known magnetic transition in ε-Fe_2O_3 [13–15]. In addition, note one more feature, specifically, the change in the $M(T)_{ZFC}$ curvature sign near 40–45 K, which is observed in all the samples. This feature is related to the presence of the fraction of particles no larger than 8 nm in size in the samples (Fig. 1). In the particles of this size, the above-described magnetic transition does not occur [32, 35], the bulk magnetic anisotropy constant decreases, and a characteristic superparamagnetic blocking temperature of up to ~80 K is observed [35]. The change in the $M(T)_{ZFC}$ curvature sign near 40–45 K reflects the transition to the blocked state of small (<8 nm) particles. Below 80 K, the effect of thermomagnetic prehistory on the $M(T)$ dependences is maximum, which is also caused by blocking of small particles.

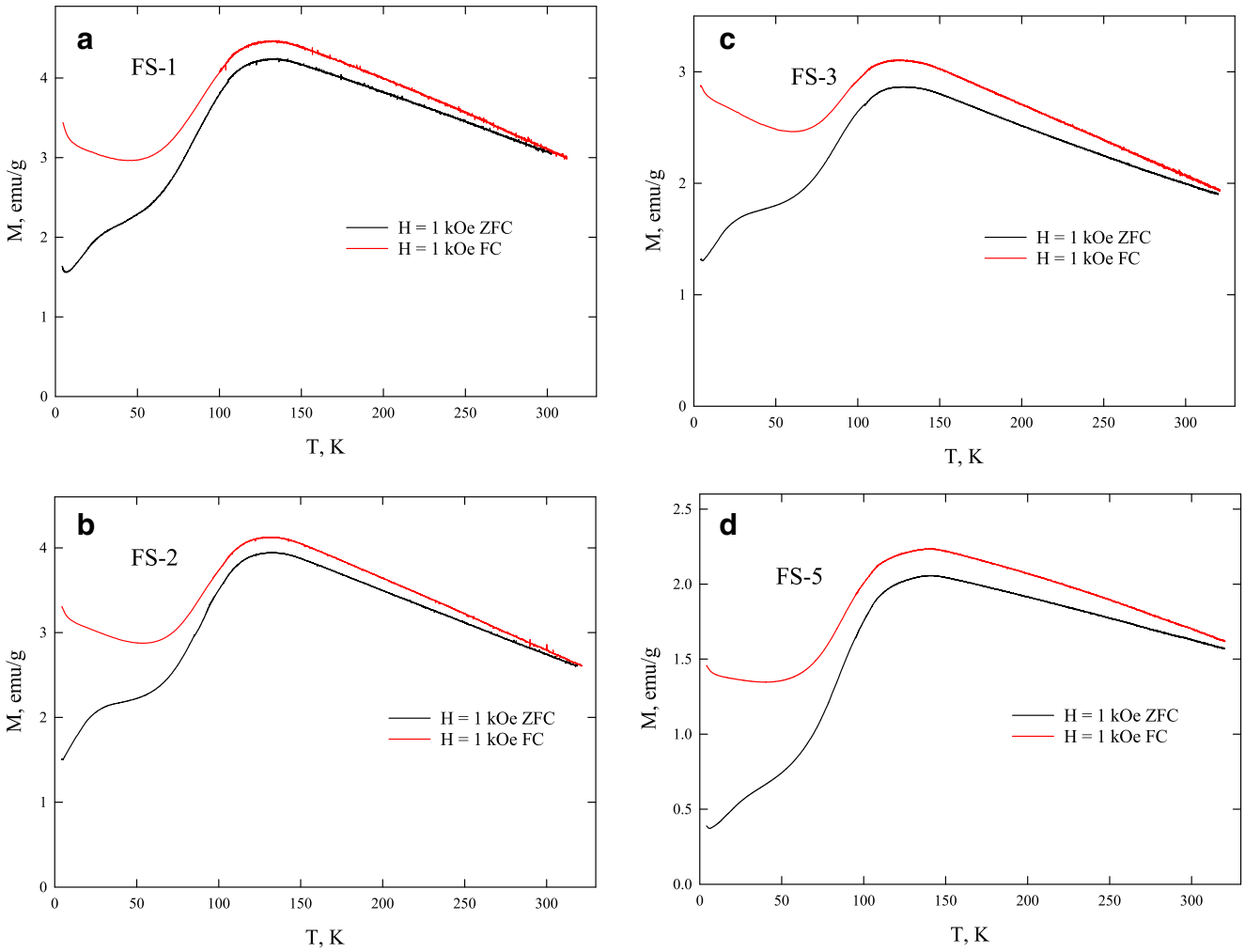

Fig. 5 ZFC and FC temperature dependences of magnetic moment for samples **a** 6FS, **b** 8FS, **c** 12FS, and **d** 16FS in a field of $H = 1$ kOe

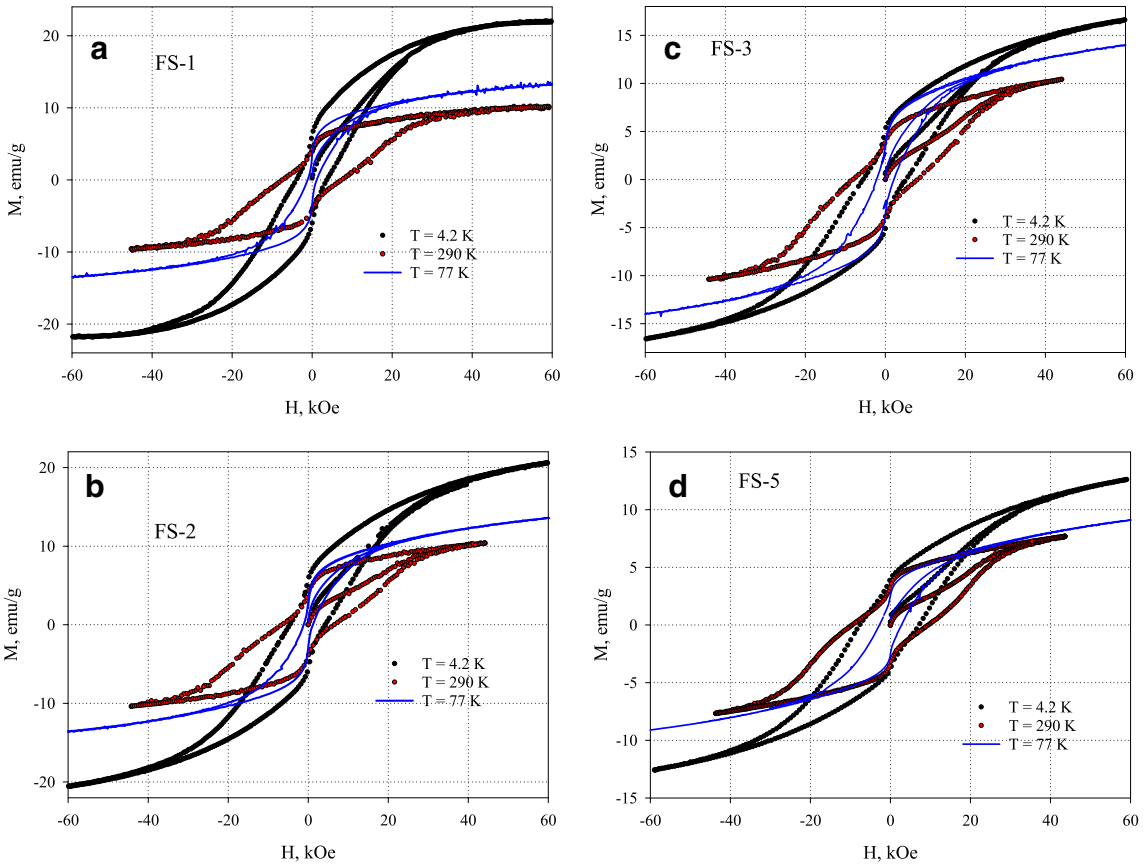

Fig. 6 Magnetic hysteresis loops for samples **a** 6FS, **b** 8FS, **c** 12FS, and **d** 16FS at the given temperatures

The $M(H)$ magnetic hysteresis loops measured at temperatures of 4.2, 77, and 300 K are illustrated in Fig. 6. It can be seen that for all the presented data, the coercivity (H_C) is minimum at 77 K, i.e., below the temperature of the magnetic transition to ε-Fe_2O_3 [13–15]. This behavior is typical of ε-Fe_2O_3, where the maximum H_C value is observed above the abovementioned magnetic transition (above 150 K). The dependences of H_C on the iron content in the samples are presented in Fig. 7. The growth of iron concentration in the samples leads to an increase in the room-temperature coercivity, which results from the particle size growth (Fig. 1).

It can be seen in Fig. 6 that the magnetic moment in external fields of stronger than ~40 kOe for sample 16FS is noticeably weaker than that for the samples with the lower iron concentrations. This agrees well with the presence of the hematite phase in this sample, which, in this case, reduces the ε-Fe_2O_3 phase fraction, so the *saturation magnetization* (M values in fields exceeding the field of irreversible magnetization behavior) decreases by about 30% in accordance with the Mössbauer spectroscopy data (Fig. 4). Indeed, hematite can be considered weakly magnetic as compared with ε-Fe_2O_3 and the magnetic response from α-Fe_2O_3 is almost indistinguishable against the background of the magnetic hysteresis loops for ε-Fe_2O_3. The $M(T)$ dependences in Fig. 4 contain no anomalies near the Morin point for hematite (≈260 K), which is reasonable to explain by the well-known fact that the Morin point of nanosized hematite particles shifts to the low-temperature region [36] and is absent for particles of about 20–40 nm in size [37].

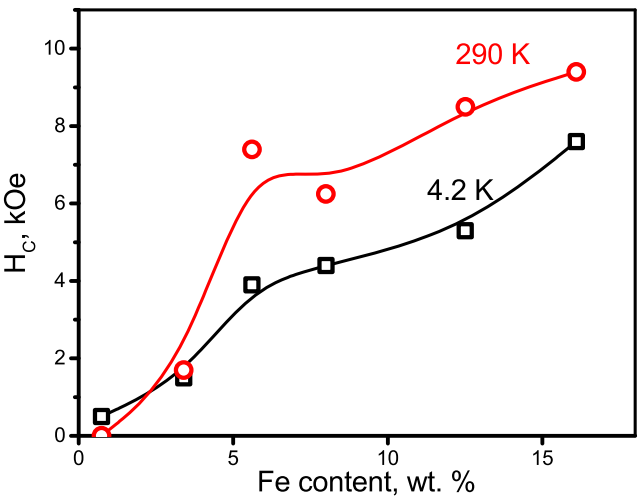

Fig. 7 Coercivities at room temperature and 4.2 K vs total iron ion content in the system

Thus, analysis of the magnetic properties of the ε-Fe_2O_3 samples obtained by multiple silica gel impregnations proves the presence of the ε-phase and formation of hematite at iron contents over 12%.

4 Conclusions

It was shown that the multiple sequential incipient wetness impregnation of silica gel with the aqueous solution of iron(II) sulfate heptahydrate and subsequent annealing at 900 °C lead to an increase in the iron content in the samples and growth of ε-Fe_2O_3 particles. According to the data obtained using different techniques (Mössbauer spectroscopy and X-ray diffraction analysis), at an iron content of ~6 wt%, the hematite phase forms and the phase transition ε-$Fe_2O_3 \rightarrow \alpha$-$Fe_2O_3$ occurs. The estimation of the critical particle size corresponding to the transition of ε-Fe_2O_3 to the more thermodynamically stable iron oxide form (α-Fe_2O_3) is 35–40 nm. At iron ion concentrations of 6–12 wt%, the α-Fe_2O_3 phase fraction is insignificant (not more than 5%; i.e., the ε-Fe_2O_3 fraction is 95%). As the iron concentration increases to 16 wt%, the hematite phase fraction attains one third. The results obtained allow us to conclude that the condition for forming the ε-Fe_2O_3/SiO_2 sample without other iron oxide polymorphs is the spatial stabilization of iron-containing particles by means of their interaction with the carrier surface for limiting the agglomeration and iron atom transport between particles.

Acknowledgments The work was supported by the Russian Science Foundation (Grant No. 17-12-01111).

Compliance with Ethical Standards

Conflict of interests The authors declare that they have no conflict of interest.

References

1. Chu, Y., Pan, Q.: Three-dimensionally macroporous Fe/C nanocomposites as highly selective oil-absorption materials. ACS Appl. Mater. Interfaces. **4**, 2420–2425 (2012). https://doi.org/10.1021/am3000825
2. Somorjai, G.A., McCrea, K.: Roadmap for catalysis science in the 21st century: a personal view of building the future on past and present accomplishments. Appl. Catal. A Gen. **222**, 3–18 (2001). https://doi.org/10.1016/S0926-860X(01)00825-0
3. Shuvaeva, M.A., Nuzhdin, A.L., Martyanov, O.N., Bukhtiyarova, G.A.: Benzylation of benzene by benzyl chloride over silica-supported iron sulfate catalysts. Mendeleev Commun. **24**, 231–232 (2014). https://doi.org/10.1016/j.mencom.2014.06.015
4. Booker, N.A., Keir, D., Priestley, A.J., Ritchie, C.B., Sudarmana, D.L., Woods, M.A.: Sewage clarification with magnetite particles. Water Sci. Technol. **23**, 1703–1712 (1991)
5. Seil, J.T., Webster, T.J.: Antimicrobial applications of nanotechnology: methods and literature. Int. J. Nanomedicine. **7**, 2767–2781 (2012). https://doi.org/10.2147/IJN.S24805
6. Gupta, A.K., Gupta, M.: Synthesis and surface engineering of iron oxide nanoparticles for biomedical applications. Biomaterials **26**, 3995–4021 (2005). https://doi.org/10.1016/j.biomaterials.2004.10.012
7. Lu, A.-H., Salabas, E.L., Schüth, F.: Magnetic nanoparticles: synthesis, protection, functionalization, and application. Angew. Chemie Int. Ed. **46**, 1222–1244 (2007). https://doi.org/10.1002/anie.200602866
8. Sakurai, S., Kuroki, S., Tokoro, H., Hashimoto, K., Ohkoshi, S.: Synthesis, crystal structure, and magnetic properties of ε-InxFe2–xO3 nanorod-shaped magnets. Adv. Funct. Mater. **17**, 2278–2282 (2007). https://doi.org/10.1002/adfm.200600581
9. Tronc, E., Chanéac, C., Jolivet, J.P.: Structural and magnetic characterization of ε-Fe2O3. J. Solid State Chem. **139**, 93–104 (1998). https://doi.org/10.1088/0953-8984/23/12/126003
10. Gich, M., Roig, A., Taboada, E., Molins, E., Bonafos, C., Snoeck, E.: Stabilization of metastable phases in spatially restricted fields: the case of the Fe2O3 polymorphs. Faraday Disc. **136**, 345 (2007). https://doi.org/10.1039/b616097b
11. Sakurai, S., Namai, A., Hashimoto, K., Ohkoshi, S.-I.: First observation of phase transformation of all four Fe2O3 phases ($\gamma \rightarrow \varepsilon \rightarrow \beta \rightarrow \alpha$-phase). J. Am. Chem. Soc. **131**, 18299–18303 (2009). https://doi.org/10.1021/ja9046069
12. Jin, J., Ohkoshi, S., Hashimoto, K.: Giant coercive field of nanometer-sized iron oxide. Adv. Mater. **16**, 48–51 (2004). https://doi.org/10.1002/adma.200305297
13. Sakurai, S., Jin, J., Hashimoto, K., Ohkoshi, S.: Reorientation phenomenon in a magnetic phase of ε-Fe2O3 nanocrystal. J. Phys. Soc. Japan **74**, 1946–1949 (2005). https://doi.org/10.1143/JPSJ.74.1946
14. Gich, M., Roig, A., Frontera, C., Molins, E., Sort, J., Popovici, M., Chouteau, G., Martín y Marero, D., Nogués, J.: Large coercivity and low-temperature magnetic reorientation in ε-Fe_2O_3 nanoparticles. J. Appl. Phys. **98**, 44307 (2005). https://doi.org/10.1063/1.1997297
15. Tseng, Y.C., Souza-Neto, N.M., Haskel, D., Gich, M., Frontera, C., Roig, A., Van Veenendaal, M., Nogués, J.: Nonzero orbital moment in high coercivity ε-Fe2O3 and low-temperature collapse of the magnetocrystalline anisotropy. Phys. Rev. B - Condens. Matter Mater. Phys. **79**, 1–6 (2009). https://doi.org/10.1103/PhysRevB.79.094404
16. Yakushkin, S.S., Bukhtiyarova, G.A., Martyanov, O.N.: Formation conditions of a magnetically ordered phase ε-Fe2O3. A FMR in situ study. J. Struct. Chem. **54**, 876–882 (2013). https://doi.org/10.1134/S0022476613050065
17. Zboril, R., Mashlan, M., Barcova, K., Vujtek, M.: Thermally induced solid-state syntheses of γ-Fe2O3 nanoparticles and their transformation to α-Fe2O3 via ε-Fe2O3. Hyperfine Interact. **139**(140), 597–606 (2002). https://doi.org/10.1023/A:1021226929237
18. Ding, Y., Morber, J.R., Snyder, R.L., Wang, Z.L.: Nanowire structural evolution from Fe3O4 to ε-Fe2O3. Adv. Funct. Mater. **17**, 1172–1178 (2007). https://doi.org/10.1002/adfm.200601024
19. Tadić, M., Spasojević, V., Kusigerski, V., Marković, D., Remškar, M.: Formation of ε-Fe2O3 phase by the heat treatment of α-Fe2O3/SiO2 nanocomposite. Scr. Mater. **58**, 703–706 (2008). https://doi.org/10.1016/j.scriptamat.2007.12.009
20. Popovici, M., Gich, M., Nižňanský, D., Roig, A., Savii, C., Casas, L., Molins, E., Zaveta, K., Enache, C., Sort, J., de Brion, S., Chouteau, G., Nogués, J.: Optimized synthesis of the elusive ε-Fe2O3 phase via sol−gel chemistry. Chem. Mater. **16**, 5542–5548 (2004). https://doi.org/10.1021/cm048628m